Eur. Phys. J. D **59**, 291–300 (2010)
DOI: 10.1140/epjd/e2010-00148-x

THE EUROPEAN PHYSICAL JOURNAL D

Regular Article

A controllable double-well optical trap for cold atoms (or molecules) using a binary π-phase plate: experimental demonstration and Monte Carlo simulation

R.W. Mu[1,2], Z.L. Wang[1], Y.L. Li[2], X.M. Ji[2], and J.P. Yin[1,a]

[1] State Key Laboratory of Precise Spectroscopy, Department of Physics, East China Normal University, 200062 Shanghai, P.R. China
[2] Science College, Nantong University, 226007 Jiangsu province, P.R. China

Received 10 August 2009 / Received in final form 18 December 2009
Published online 26 May 2010 –

Abstract. We experimentally demonstrate a practical scheme to form a controllable double-well optical dipole trap for cold atoms (or cold molecules), and give some experimental results as well as the fabrication method of a binary π-phase plate. The dependence of the double-well characteristics on the phase etching error of the π-phase plate and the evolution of the double-well optical trap from two wells to a single one are studied both theoretically and experimentally, and the experimental results are consistent with the theoretical prediction. Furthermore, the dynamic process of loading and splitting of cold ^{87}Rb atoms from a standard magneto-optical trap (MOT) into our controllable double-well one are studied by Monte Carlo simulations. Our study shows that the loading efficiency of cold atoms from the standard MOT into our single-well trap can reach 100%, and the relative atomic density will be reduced from 1.0 to ∼0.5 during the evolution of our double-well trap, in which the temperature of cold atoms is reduced from 20 μK to ∼15 μK. In final, some potential applications of our controllable double-well optical trap in atom and molecule optics are briefly discussed.

1 Introduction

Recently, Yin et al. proposed several controllable double-well magneto-optical traps and double-well magnetic traps for cold atoms by using current-carrying wires, which can be used to realize the continuous evolution of double-well magnetic trap from two wells to a single one by changing both the direction and magnitude of the current in the wire or the additional bias magnetic field [1–3]. These controllable double-well traps can be used to prepare two-species magneto-optical trap (MOT) for cold atoms or to study their cold collision properties, even to realize a double-well Bose-Einstein condensation (BEC). In 2002, Thomas et al. proposed a scheme to realize double-well BEC by using double-well Ioffe-Pritchard (IP) magnetic trap based on time-averaged orbiting potential (TOP) [4]. In the same year, Walraven's group realized the first double-well ^{87}Rb BEC by using double-well TOP magnetic trap, and obtained a pure condensate with a number of 4×10^4 atoms and studied the vibration effect of axial center-of-mass motion of BEC in the double wells [5]. In recent years, in particular, the applied researches on various controllable double-well magnetic, optical or magneto-optical traps have become one of hot subjects in the fields of ultracold atomic physics, atom optics and quantum optics [6–14]. For instance, they can be used to study the two-species MOT, cold collisions between two atomic samples, properties of double-well atomic BECs, matter-wave interference of trapped atoms and quantum entanglement between two atomic assemblies, etc.

It is well-known that a single optical dipole trap composed of a focused far-red-detuned Gaussian beam can be conveniently used to realize high-efficient loading, trapping and manipulating of cold atoms (or molecules) as well as optical-potential evaporative cooling, while a controllable double-well optical trap can be used to study collision properties between cold atoms (or molecules), quantum tunnel effect between two wells and its atom interference [6,15], or to trap and manipulate cold molecules and prepare novel optical lattices, even to realize molecular BEC [16–19] and study BEC properties in optical lattice [20–23]. Therefore, it would be interesting and worthwhile to generate and study a novel controllable double-well optical trap (DWOT), both theoretically and experimentally. More recently, we proposed a new scheme to form a controllable DWOT for cold atoms (or molecules) and obtained some worthwhile theoretical results [24]. In this paper, the fabrication of the binary π-phase plate is briefly introduced and the generation of controllable DWOT is demonstrated experimentally. The

[a] e-mail: jpyin@phy.ecnu.edu.cn

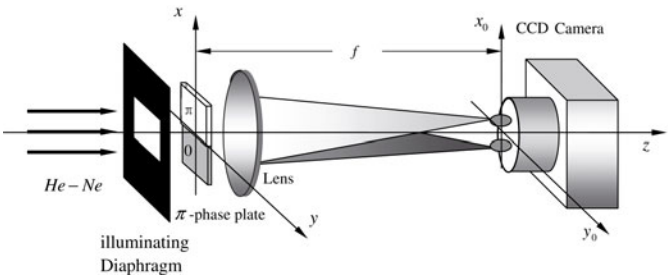

Fig. 1. The experimental setup to generate a controllable double-well optical dipole trap.

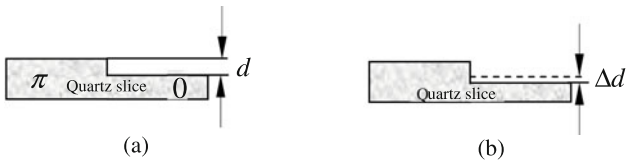

Fig. 2. (a) An ideal π-phase plate with a standard etching depth d, and (b) a real π-phase plate with an etching depth error Δd.

influence of the etching depth error of the binary π-phase plate on the performance and evolution of double-well trap are analyzed, and some experimental results consistent with theoretical calculations are obtained. Also, we study the dynamic loading and splitting processes of cold ^{87}Rb atoms from a standard MOT into our controllable double-well one by Monte Carlo simulations, and obtain some simulated results consistent with theoretical prediction. Finally, some potential applications of our controllable DWOT are briefly discussed, and the main results and conclusions are summarized.

2 Experimental method and results

The scheme of a controllable DWOT is generated by an illuminating aperture with a side length of $2a = 2$ mm, a binary π-phase plate and an ordinary positive lens with a focal length of $f = 500$ mm illuminated by a He–Ne laser beam, as shown in Figure 1. Here the binary π-phase plate is formed by two square phase sheets with a side length $2a$ and a phase difference π. When a He–Ne laser field passes through the binary π-phase plate and is focused by the lens, an optical dipole trap with two wells for cold atoms (or molecules) will be produced near the focal point of the lens. And the intensity distribution of the generated double wells near the focal point of the lens can be measured by using a CCD camera. The basic principle to produce a controllable DWOT and to evolve a double-well trap into a single-well one can be found in reference [24].

To generate the DWOT, we choose a quartz slice with a refractive index of $n = 1.46$ as a substrate of the π-phase plate and a He–Ne laser with a wavelength of $\lambda = 632.8$ nm as an incident light field. The theoretical value of the standard etching depth in the 0 phase region of the phase plate is $d = \frac{\lambda}{2(n-1)} = 687.8$ nm (see Fig. 2). In our DWOT experiment, a JR-2B ion etching machine is used to fabricate our binary π-phase plate. Five π-phase plates are etched by choosing different etching time, and the corresponding etching depth is measured by using Dektek 3st step instrument, and the etching depths of the five phase plates are 453.0, 491.3, 608.1, 649.8 and 669.6 nm. Therefore, the differences Δd between the real etching depth and the standard etching depth d are -234.8, -196.5, -79.7, -38.0 and -18.2 nm, respectively, as shown in Figure 2, and the corresponding phase errors $\Delta\varphi$ are -1.0724, -0.8977, -0.3643, -0.1736 and -0.083 rad, respectively.

In our experiment, the illuminating aperture is chosen as a $2a \times 2a = 2$ mm $\times$ 2 mm square one, and its half side length is $a = 1$ mm. The intensity distributions of the generated double wells are measured by using a XC-ST50CE model CCD camera in the focal plane of the lens with a focal length of $f = 500$ mm and the space resolution (i.e., the pixel size) of the CCD camera is 8.6×8.3 μm^2. We add a proper attenuator in the light path to limit the exposure to be below its saturation value in order to avoid pixel saturation. To obtain a clear image of the DWOT, the distance between the illuminating aperture and the binary π-phase plate must be chosen as small as possible. The experimental results of the observed double-well images and their 2D intensity distribution are shown in Figure 3, and the observed maximal relative intensity of each pair of optical wells and the positions of the double-well centers as well as their spacing are shown in Table 1.

It can be seen from Table 1 that when the phase difference of the etched phase plate is not an ideal π, the intensity distribution of the DWOT will be changed. With the increase of the phase error $\Delta\varphi$, the intensity of the left optical well will be decreased, while one of the right well will be increased. Accordingly, the difference $I_{R\max} - I_{L\max}$ between the maximum intensities of the two optical wells increases with the phase error $\Delta\varphi$. However, the change of the distance between two-well centers is very small. Note that the positions of the two-well centers and the distances between the two-well centers in Table 1 have an estimated error of half a pixel (± 4.3 μm).

If the phase plate is moved along the x-direction, a double-well optical trap will be gradually evolved as a single-well one. In our experiment, the phase plate with an etching depth of 704.5 nm was used and the corresponding phase error is $\Delta\varphi = 0.0763$ rad. When the moving distances of the phase plate are 0.0, 0.3, 0.55, 0.7 and 1.0 mm, five images from the evolution of a double-well trap to a single-well one and their 2D intensity distributions are observed, and the results are shown in Figure 4. Table 2 gives some measured data of our double-well trap, such as the maximum relative intensities of each pair of optical wells, the position of the two-well centers and the distance between two-well centers. Here the positions of the two-well centers in Table 2 have also an estimated error of half a pixel (± 4.3 μm).

We can find from Table 2 and Figure 3 that with the increase of the moving distance t of the π-phase plate, the maximum intensities of the two optical wells is first

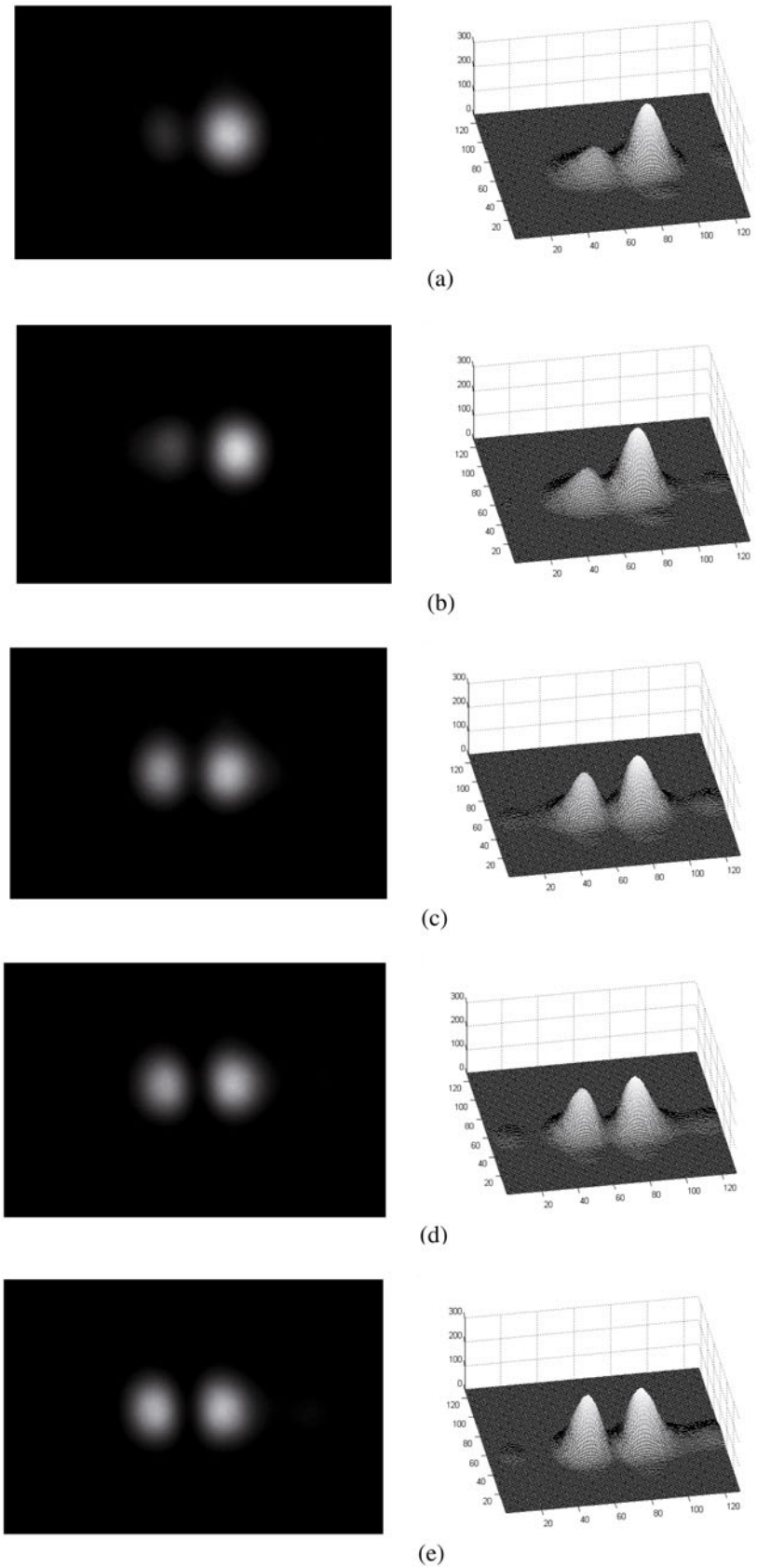

Fig. 3. The experimental results on the evolution of 2D intensity distribution of the double-well optical trap for the phase error (a) $\Delta\varphi = -1.0724$, (b) $\Delta\varphi = -0.8977$, (c) $\Delta\varphi = -0.3643$, (d) $\Delta\varphi = -0.1736$, and (e) $\Delta\varphi = -0.0830$. Here the horizontal and vertical axes (unit: pixels) are the x- and y-directions, respectively.

Table 1. The measured results of the DWOT parameters.

	$\Delta\varphi = -1.0724$		$\Delta\varphi = -0.8977$		$\Delta\varphi = -0.3643$		$\Delta\varphi = -0.1736$		$\Delta\varphi = -0.0830$	
	Left well	Right well	Left well	Right well	Left well	Right well	Left well	Right well	Left well	Right well
Maximal relative intensity	94	253	110	250	163	218	171	208	188	203
Difference between the two maximal relative intensities	159		140		55		37		15	
Position of the two-well centers (pixels)	54	81	59	86	48	75	45	73	58	86
Distance between the two-well centers (μm)	232.2		232.2		232.2		240.8		240.8	

decreased, and then two wells are combined as a single-well and its intensity is increased. However, the difference $I_{L\max} - I_{R\max}$ between the maximum relative intensities of the two optical wells is gradually increased, and the distance between the two-well centers is decreased with the increase of the moving distance t.

3 Analysis and discussion

In our experiment, we find that the etching depth error of the π-phase plate mainly results in the change of the intensity distribution of the DWOT. Therefore, we analyze the influence of the etching depth error of the π-phase plate on the parameters of the DWOT and compared them with the experimental results. In reference [24], we analyze the difference between the intensity distributions of the DWOT formed by a Gaussian beam or a plane-wave light, and found that when the beam waist w_0 is small, the difference of the intensity distributions from the above two incident beams is large. However, when $w_0 \geq \sqrt{2}a$, the intensity distributions of the DWOT formed by the TEM_{00}-mode Gaussian beam is very close to that formed by the plane-wave light, and the smaller the beam waist w_0 is, the greater the difference between two beam models is. Since our optical system satisfies the condition $w_0 \geq \sqrt{2}a$, the plane-wave illumination model is used in our theoretical analysis.

The phase difference of the fabricated π-phase plate used in the experiment is not an accurate π due to the existence of the etching depth error, we suppose that the resulting phase error is $\Delta\varphi$, the transmittance function of the π-phase plate can be expressed as

$$g(x,y) = \mathrm{rect}\left[\frac{x-a}{2a}, \frac{y}{2a}\right] - \mathrm{rect}\left[\frac{x+a}{2a}, \frac{y}{2a}\right]\exp(i\Delta\varphi), \quad (1)$$

where $\mathrm{rect}(x)$ is the rectangular function. Assuming that the focal length of the lens is f, when the optical system, as shown in Figure 1, is illuminated by a plane wave with a wavelength λ and an amplitude a propagated along the z-direction, according to Fresnel diffraction theory, the distribution of the light disturbance on the x_0oy_0 plane can be given by:

$$U(x_0,y_0,z) = \frac{A}{\lambda z}\int_{-a}^{a}\int_{-a}^{a} g(x,y) \times \exp\left\{\frac{i\pi}{\lambda}\left[(x^2+y^2)\left(\frac{1}{z}-\frac{1}{f}\right) - \frac{2(xx_0+yy_0)}{z}\right]\right\} dx\,dy. \quad (2)$$

Here z is the distance from the lens to the x_0oy_0 plane, and some constant phase factors are not important and can be neglected. Equation (2) is so complicated that the intensity distribution on an arbitrary plane (x_0, y_0, z) can not be written with an analytical expression. However, the intensity distribution on the focal plane $(x_0, y_0, z = f)$ can be given by an analytical formula as follows:

$$I_f = |U(x_0,y_0,f)|^2 = \frac{16A^2a^4}{(\lambda f)^2}\,\frac{\sin^2(\pi a x_0/\lambda f)\sin^2(\pi a x_0/\lambda f - \Delta\varphi/2)}{(\pi a x_0/\lambda f)^2} \times \frac{\sin^2(2\pi a y_0/\lambda f)}{(2\pi a y_0/\lambda f)^2}. \quad (3)$$

It can be seen from equation (3) that the intensity distribution of the DWOT will be changed owing to the existence of the phase error $\Delta\varphi$, which is produced by the etching depth error of the π-phase plate. We study the dependence of the difference $(I_{R\max} - I_{L\max})$ between the two-well maximum relative intensities on the phase error $\Delta\varphi$, and find that the theoretical results are in good agreement with our experimental results (see Tab. 1), and the intensity difference $(I_{R\max} - I_{L\max})$ is linearly dependent on the phase error $\Delta\varphi$ and given by

$$I_{R\max} - I_{L\max} = A + B\Delta\varphi, \quad (4)$$

where $A = 0.000731$ and $B = -0.94073$ are the two fitting parameters.

From equation (3), we calculate the intensity distribution of our double-well trap on the focal plane in the x-direction for the different phase error (such as $\Delta\varphi = -0.0830$, -0.1736, -0.3643, -0.8977 and -1.0742) and fit these theoretical results with our experimental measured data, and the results are shown in Figure 5. It can

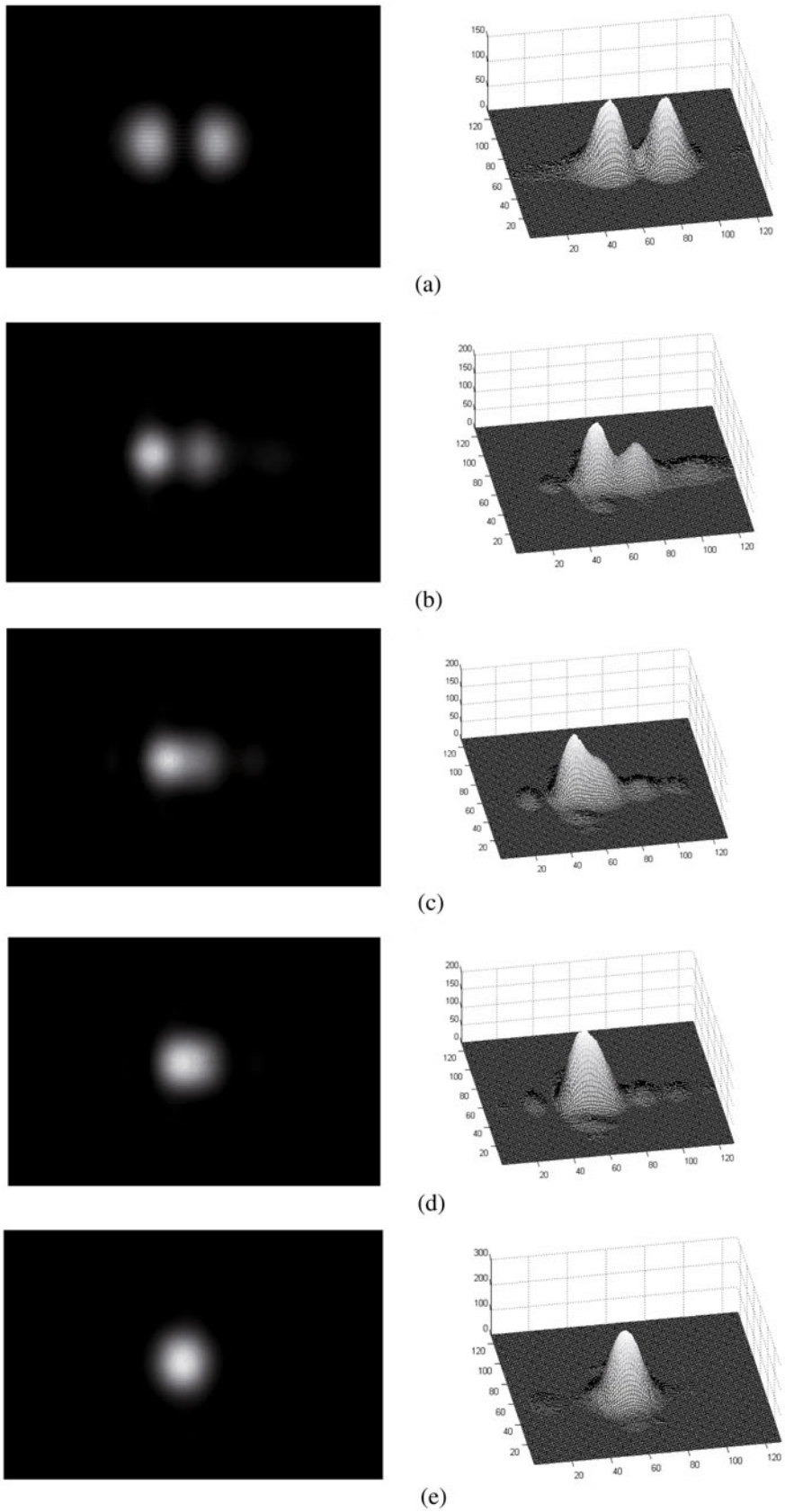

Fig. 4. The experimental results on the evolution of our optical dipole trap from a double-well trap to a single-well one for the moving distance of the π-phase plate (a) $t = 0.00$ mm, (b) $t = 0.30$ mm, (c) $t = 0.55$ mm, (d) $t = 0.70$ mm, and (e) $t = 1.00$ mm. Here the horizontal and vertical axes (unit: pixels) are the x- and y-directions, respectively.

Table 2. The experimental results of the evolution of our double-well trap to single-well one.

	$t = 0.00$ mm		$t = 0.30$ mm		$t = 0.55$ mm		$t = 0.70$ mm
	Left well	Right well	Left well	Right well	Left well	Right well	Single-well optical trap
Maximal relative intensity	186	174	168	152	151	129	179
Difference between the two maximal relative intensities	12		16		22		0
Position of the two-well center (pixels)	54	82	56	81	58	77	62
Distance between two well centers (μm)	240.8		215.0		163.4		0

$$I_f(x,y) = \frac{4P_0a^4}{(\lambda f)^2}\,\frac{\cos^2(2\pi ax/\lambda f - \Delta\varphi/2) + \cos^2(\Delta\varphi/2) - 2\cos^2(2\pi ax/\lambda f - \Delta\varphi/2)\cos(\Delta\varphi/2)\cos(2\pi tx/\lambda f)}{(2\pi ax/\lambda f)^2}\,\frac{\sin^2(2\pi ay/\lambda f)}{(2\pi ay/\lambda f)^2}. \tag{5}$$

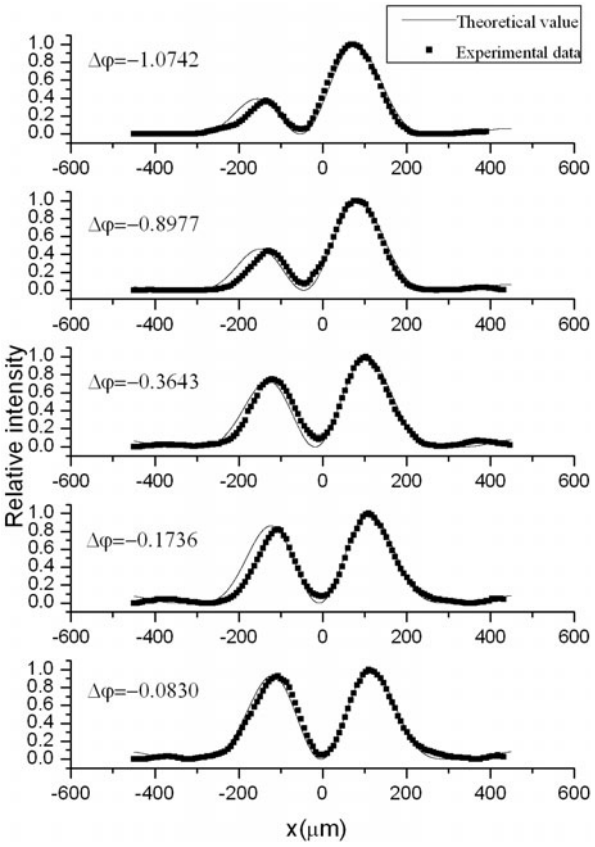

Fig. 5. 1D intensity distribution of our double-well trap in the x-direction on the focal plane for the different phase error $\Delta\varphi = -1.0724$, -0.8977, -0.3643, -0.1736, and -0.0830. The solid lines are the theoretically calculated results, and the data points are the experimentally measured ones.

be seen from Figure 5 that with the increase of $\Delta\varphi$, the positions of the two well centers are both shifted to the left, and the height of the left optical well is gradually lowered, and these experimental results are nearly consistent with the theoretical curves.

We also measure and calculate the relative intensity distributions of our DWOTs before and after the focal plane ($x_0, y_0, z = f$) for different phase error ($\Delta\varphi = -0.0830$, -0.1736, -0.3643, -0.8977 and -1.0742), and obtain the relative intensity distributions of our left and right wells in the z-direction around the focal plane, as shown in Figure 6. It is clear from Figure 6 that the experimental results are basically consistent with our theoretically calculated ones, and the phase error of the π-phase plate only influence the relative intensities of our double wells, but don't influence their intensity distributions in the z-direction, and the smaller the phase error is, the smaller the relative intensity difference between our left and right optical wells is. This shows that the phase error from the etching depth of our phase plate don't cause the optical potential deformation in the non-focal plane, that is, the phase error don't seriously influence the z-dependence of the trapping potential, which is similar to the case in the x-direction (see Fig. 5).

Moreover, our theoretical calculation shows that the intensity gradient in the z-direction is proportional to $(a/f)^6$, here a/f is the relative aperture of our lens system. Our experimental results also demonstrate this point. The relative aperture is very small ($a/f = 1/500$) in our experiment due to the limitation of the CCD resolution, so the intensity gradient of our DWOPs in the z-direction is very small. In fact, we can choose a larger relative aperture (such as $a/f = 1/40$ in our simulation, even a larger value) to greatly increase the intensity gradient of our DWOPs and reduce its longitudinal size in the z-direction in a real atom trapping experiment.

If the binary π-phase plate is moved along the x-direction with a moving distance t, the intensity distribution on the focal plane is rewritten as

see equation (5) above.

The intensity at the focal point of the lens can be derived from equation (5), and is given by: $I_{f0} = 4P_0a^4[\sin^2(-\Delta\varphi/2) + (t/a)^2]/(\lambda f)^2$ and $P_0 = 4A^2a^2$, which shows that the intensity at the focal point of the

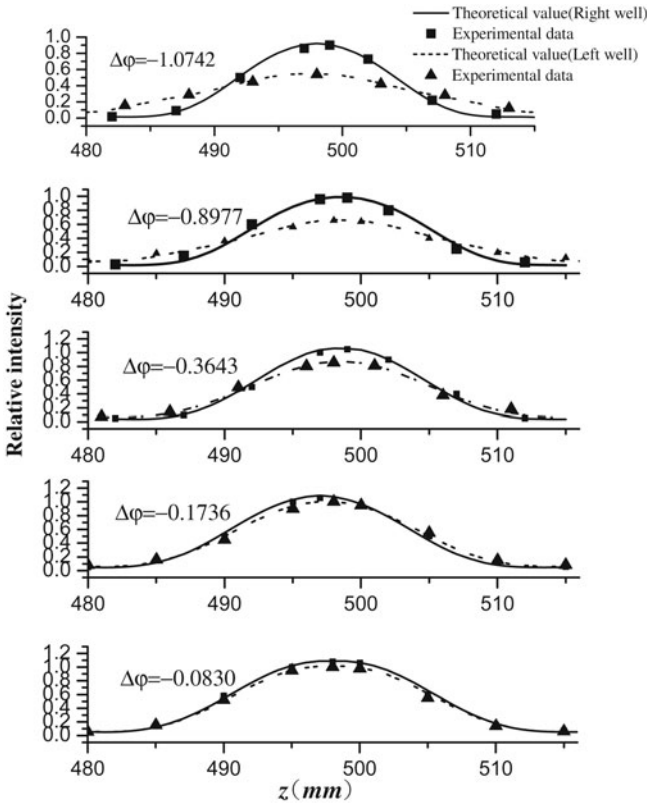

Fig. 6. 1D intensity distribution of our double-well trap in the z-direction for the different phase error $\Delta\varphi = -1.0724$, -0.8977, -0.3643, -0.1736, and -0.0830. The meanings of the lines and data points are shown in the top right corner.

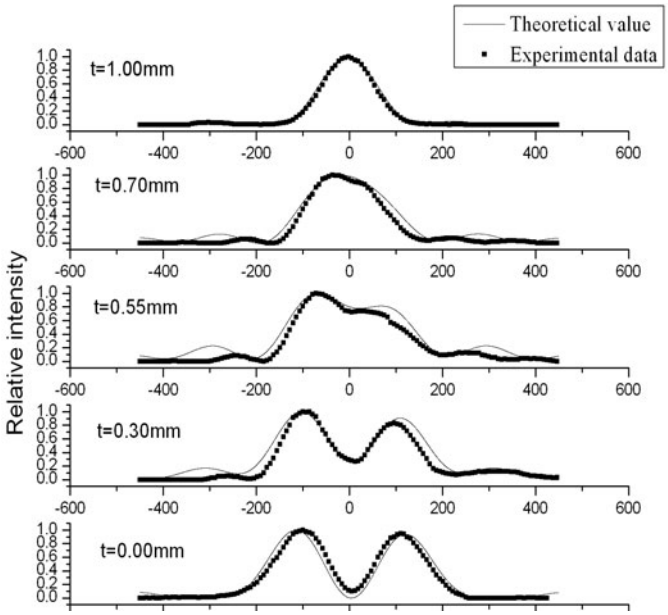

Fig. 7. 1D intensity distribution of the evolution of our optical dipole trap from a double-well trap to a single-well one for the moving distance of the π-phase plate (a) $t = 0.00$ mm, (b) $t = 0.30$ mm, (c) $t = 0.55$ mm, (d) $t = 0.70$ mm, and (e) $t = 1.00$ mm. The meanings of the solid line and data points are the same as ones in Figure 5.

lens is related to the phase error $\Delta\varphi$ and the moving distance t of the phase plate. As long as $\Delta\varphi \neq 0$, the intensity at the focal point of the lens is not zero, that is, the position of the completely destructive interference point will be not at the focal point and deflected away from the origin due to the existence of $\Delta\varphi$. When $\Delta\varphi$ is constant, the intensity at the focal point will be increased with the increase of the moving distance t.

According to equation (5), we theoretically calculate and experimentally measure the intensity distributions of our double-well trap in the evolution process from the DWOT to the single-well optical trap (SWOT) when the moving distance t of the π-phase plate are 0.00, 0.30, 0.55, 0.70 mm and 1.00 mm respectively, and the phase error of the π-phase plate is 0.0765. All the results are shown in Figure 7. We can find from Figure 7 that with the increase of the moving distance t, the distance $\Delta x_{\max}$ between the two-well centers will be gradually reduced. In particular, when the moving distance is $t = 0.7$ mm, the two optical wells are nearly combined into one well, and when $t = a$, the DWOT will be evolved as the SWOT. In this case, the intensity of the SWOT is about twice of the DWOT. These experimental results are nearly consistent with the theoretical ones. It is clear that our theoretical model and all experimentally measured results for our double-well trap are correct and reliable.

4 Monte Carlo simulations

We use Monte Carlo method to simulate and study the dynamic loading process of cold ^{87}Rb atoms from the MOT into our single-well trap and the splitting process of cold atoms from a single-well to a double one. In our simulations, the initial positions and velocities of cold atoms in the MOT are described by the Gaussian distribution respectively, and the stochastic variables are the initial position, velocity and its motional direction of cold atoms. Each atom, according to Newton's equations of motion, moves in our real light field, and the collisions between cold atoms are neglected for the sake of convenience and due to its lower atomic density. The simulation parameters are $\lambda = 1.06$ μm, $P = 4$ W, $a = 0.50$ mm and $f = 20$ mm. In our Monte Carlo simulations, since the loading process of cold atoms should be adiabatic, the moving distance Δt of the π-phase plate per step and its speed should be very small, here Δt is taken as 0.1 μm. Our simulation is performed as follows: cold ^{87}Rb atoms with a temperature of 20 μK and a number of $N_0 = 1 \times 10^4$ are first prepared in the micro-MOT, and loaded into the single-well trap ($t = 0.50$ mm) of our scheme. Then, cold atomic ensemble in the single-well trap is split and loaded into the double-well trap by moving the phase plate from $t = 0.50$ mm to 0.00 mm. Figure 8 shows the loading and splitting processes of cold atomic cloud in the xoy and xoz planes from a single-well trap to a double-well one. We can see from Figure 8(a) that a cold atomic cloud is first evolved as a longed one along the x-direction with the reduction of t, and when $t = 0.33$ mm, a long atomic cloud is split into

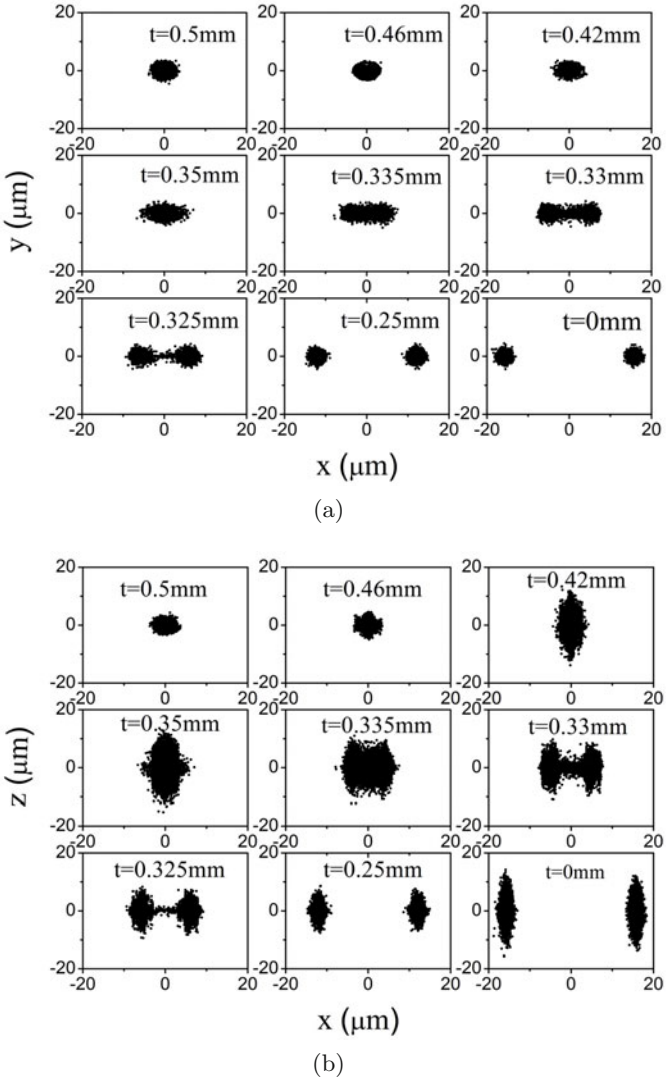

Fig. 8. Results of Monte Carlo simulations: the evolution of cold atomic cloud in the (a) xoy and (b) xoz planes during the loading and splitting processes of cold atoms for the parameters: $\lambda = 1.06$ μm, $P = 40$ W, $a = 0.50$ mm, and $f = 20$ mm.

two small ones. Figure 8(b) shows that a clod cloud is first evolved as a slightly longed one along the z-direction with the reduction of t, and when $t = 0.33$ mm, a long atomic cloud is split into two small ones in the x-direction, and then the two atomic clouds are evolved as two more long ones along the z-direction as $t = 0$.

In our simulation, we assume that the cold atomic cloud in the MOT has a Gaussian spatial distribution in the beginning of the loading, and when the atomic number is N_0, the initial atomic density n_0 can be defined as the ratio of atomic number to the effective trapping volume. Similarly, we assume that the cold atomic cloud in the SWOT or DWOT has a Gaussian spatial distribution, and the atomic density n in the SWOT or DWOT can also be defined as the ratio of atomic number to the effective trapping volume. Figure 9 shows the evolution of the relative atomic density (n/n_0) and the temperature

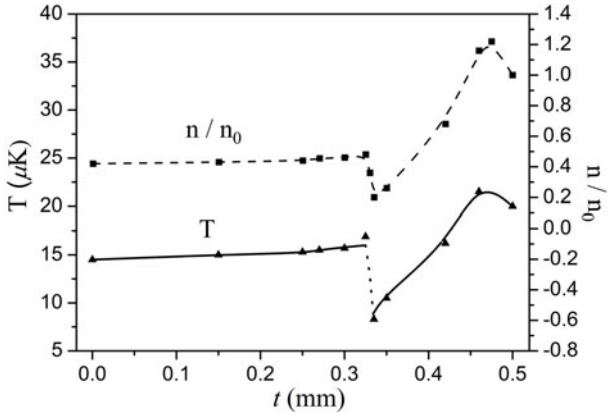

Fig. 9. The dependence of the normalized atomic density and its temperature on the moving distance t of the π-phase plate. For the normalized atomic density n/n_0, the solid line is from the simulated results; for the temperature T, the solid line is from the theoretically prediction, and the data points are from the simulated results.

of cold atoms. We can find from Figure 9 that when t is decreased from 0.50 mm to about 0.45 mm, the relative atomic density is increased from 1.0 to 1.2 due to the compression of cold atomic cloud in the loading process from the MOT to a single-well trap. When t is decreased from 0.45 mm to 0.335 mm, the relative atomic density is fast decreased from 1.2 to 0.22 due to the expansion of cold atomic cloud in a single-well trap, and then slightly increased from 0.22 to 0.46 within $t = 0.335 - 0.33$ mm due to the splitting and compression of the atomic cloud, and finally slowly decreased in the left (and right) well of our double-well trap from 0.46 to 0.42 as $t < 0.33$ mm due to the expansion of the atomic cloud in the z-direction.

Also, we can find from Figure 9 that the loading efficiency of cold atoms from the MOT into our single-well trap can reach 100%, because the trap is deep enough to trap all cold atoms from the MOT. When t is decreased from 0.50 mm to 0.45 mm, the temperature of cold atoms is first increased from 20 μK to 22.8 μK due to the adiabatic compress of cold atomic cloud in a single-well, and then when t is decreased from 0.45 mm to 0.335 mm, the temperature of cold atoms is fast decreased from 22.8 μK to 7.2 μK due to the adiabatic expansion of cold atomic cloud in a single-well, and then suddenly increased from 7.2 μK to 13.5 μK within $t = 0.335-0.33$ mm due to the non-adiabatic splitting, and finally slowly increased from 13.5 μK to 14.5 μK as $t < 0.33$ mm due to the slower adiabatic expansion of the atomic cloud in the z-direction. The solid line in Figure 8 shows the evolution of atomic temperature T calculated by the oscillation frequency of cold atoms in our trap. Note that here T is the total temperature, which is calculated by $T_i = m\omega_i^2 x_i^2/k_B$ $(i = x, y, z)$, here m is the atomic mass, ω_i is the oscillation frequency in the i $(i = x, y$ and $z)$ direction, and k_B is Boltzmann coefficient. It is clear from Figure 9 that the simulated results are in good agreement with the theoretical prediction in the adiabatic expansion processes (i.e., $t = 0.50-0.335$ mm and $0.33-0$ mm), while

$t = 0.335-0.33$ mm, there is a greater deviation between the simulated results and theoretical prediction since the splitting of cold atomic cloud is a non-adiabatic process. We also can see from Figure 9 that the phase space density of the trapped cold atoms, proportional to $nT^{-3/2}$, is kept to be nearly unchanged during the adiabatic evolution (including the adiabatic compression and expansion) processes.

5 Conclusion and outlook

In this paper, we have first introduced the experimental scheme to generate a controllable DWOT for cold atoms (or molecules), and reported the fabricating method of the binary π-phase plates and their experimental results. Also, we have analyzed the influence of the etching depth error of the phase plate on the performance and evolution of the DWOT both theoretically and experimentally, and obtained some new experimental results. Our study shows:

(1) the difference $|I_{R\max} - I_{L\max}|$ of the two well maximal intensities will be increased linearly with increasing the phase error $\Delta\varphi$;
(2) the distance $\Delta x_{\max}$ between two well centers will be decreased with the increases of $\Delta\varphi$, but the change of $\Delta x_{\max}$ is very small, even it can be neglected;
(3) when the moving distance of the phase plate is $t = a$, the DWOT will be evolved as the SWOT, and the intensity of the SWOT is about twice of the DWOT.

These experimental results are in good agreement with the theoretical calculations.

We have also studied the loading and splitting processes of cold atoms in our controllable double-well trap by Monte Carlo simulations, and obtained some simulated results consistent with theoretical prediction. Our simulation shows that the loading efficiency of cold atoms from the MOT into our single-well trap can reach 100%, and the relative atomic density is reduced from 1.0 to ~0.42, and the temperature of cold atoms is reduced from 20 μK to 14.5 μK during the evolution of our double-well trap. As compared with other optical double-well traps, our double-well one with a giant red-detuning has some new and unique advantages as follows:

(1) it is easy to efficiently load cold atoms from a MOT into our trap;
(2) it is convenient to manipulate and control cold atoms in our double-well trap so as to perform a matter-wave interference of trapped atoms;
(3) it can be used to form an all-optical atom chip or to develop a novel 2D optical lattice [24]; even to realize an all-optical double-well or two-species BEC by using optical-potential evaporative [25], etc.

However, our scheme has also some disadvantages, such as a high mechanical stability of our optical system is required when the phase plate is moving, and so on.

Further study found that if a YAG laser with a wavelength of $\lambda = 1.06$ μm and a power of 4 W is used to trap cold ^{87}Rb atoms, and when the relative aperture $\beta = a/f = 0.025$, the optical trapping potential is greater than 0.7 mK, which is far higher than the temperature (~20 μK) of cold ^{87}Rb atoms from a standard MOT. The corresponding mean photon scattering rate is lower than 1/s. So such a controllable double-well optical dipole trap has some important and wide applications in the fields of ultracold atomic and molecular physics as well as atom and molecule optics. For example, it can be used to trap cold atoms (or molecules), to study cold collisions between two atomic (or molecular) samples and interference of trapped ultracold atoms [26,27], to measure the relative phase of two BECs [28–30], or to form novel optical lattices [24] and all-optical integrated atom (or molecule) chip, and to perform quantum computing and quantum information processing [31,32], to study quantum entanglement [33,34] and nonlinear Zener tunneling [35,36], even to trap a quasi-2D BEC [37–39] or realize all-optical atomic (or molecular) double-well BECs and their BEC lattices by using optical-potential evaporative cooling [16,25,40].

This work is supported by the National Natural Science Foundation of China under Grant Nos. 10434060, 10674047, 10804031, 10904037 and 10904055; the National Key Basic Research and Development Grogram of China under grant No. 2006CB921604; the Basic Key Program of Shanghai Municipality under Grant No. 07JC14017; the Program for Changjiang Scholar and Innovative Research Team, Shanghai Leading Academic Discipline Project under Grant No. B408; and the Natural Science Foundation of Jiangsu Province, China Grant No. BK2008183.

References

1. J. Hu, J. Yin, J. Opt. Soc. Am. B **19**, 2844 (2002)
2. J. Hu, J. Yin, J. Opt. Soc. Am. B **22**, 937 (2005)
3. M. Yun, J. Yin, Opt. Lett. **30**, 696 (2005)
4. N.R. Thomas, A.C. Wilson, C.J. Foot, Phys. Rev. A **65**, 063406 (2002)
5. T.G. Tiecke, M. Kemmann, C. Buggle, I. Shvarchuck, W. von Klitzing, J.T.M. Walraven, J. Opt. B Quant. Semiclass. Opt. **5**, S119 (2003)
6. M. Albiez, R. Gati, J. Fölling, S. Hunsmann, M. Cristiani, M.K. Oberthaler, Phys. Rev. Lett. **95**, 010402 (2005)
7. T. Schumm, S. Hofferberth, L.M. Andersson, S. Wildermuth, S. Groth, I. Bar-Joseph, J. Schmiedmayer, P. Krüger, Nature Phys. **1**, 57 (2005)
8. L.G. Marcassa, G.D. Telles, S.R. Muniz, V.S. Bagnato, Phys. Rev. A **63**, 013413 (2000)
9. M. Modugno, F. Dalfovo, C. Fort, P. Maddaloni, F. Minardi, Phys. Rev. A **62**, 063607 (2000)
10. P. Öhberg, L. Santos, Phys. Rev. Lett. **86**, 2918 (2001)
11. G. Delannoy, S.G. Murdoch, V. Boyer, Phys. Rev. A **63**, 051602 (2001)
12. H.J. Wang, X.X. Yi, X.W. Ba, Phys. Rev. A **62**, 023601 (2000)
13. L. Pitaevskii, S. Stringari, Phys. Rev. Lett. **87**, 180402 (2001)
14. M.K. Olsen, J.J. Hope, Phys. Rev. A **64**, 013601 (2001)
15. M. Arndt, M. Ben Dahan, D. Guéry-Odelin, M.W. Reynolds, J. Dalibard, Phys. Rev. Lett. **79**, 625 (1997)

16. S. Jochim, M. Bartenstein, A. Altmeyer, G. Hendl, S. Riedl, C. Chin, J.H. Denschlag, R. Grimm, Science **302**, 2101 (2003)
17. M. Greiner, C.A. Regal, D.S. Jin, Nature **426**, 537 (2003)
18. T. Takekoshi, B.M. Patterson, R.J. Knize, Phys. Rev. Lett. **81**, 5105 (1998)
19. M.W. Zwierlein, C.A. Stan, C.H. Schunck, S.M.F. Raupach, S. Gupta, Z. Hadzibabic, W. Ketterle, Phys. Rev. Lett. **91**, 250401 (2003)
20. B.P. Anderson, M.A. Kasevuch, Science **282**, 1686 (1998)
21. G. Modugno, G. Ferran, G. Roati, R.J. Brecha, A. Simoni, M. Inguscio, Science **294**, 1320 (2001)
22. W. Hänsel, P. Hommelhoff, T.W. Hänsch, J. Reichel, Nature **413**, 498 (2001)
23. K.B. Dävis, M.O. Mewes, M.R. Andrews, N.J. van Druten, D.S. Durfee, D.M. Kurn, W. Ketterle, Phys. Rev. Lett. **75**, 3969 (1995)
24. Xianming Ji, Jianping Yin, J. Opt. Soc. Am. B **22**, 1737 (2005)
25. Jianping Yin, Phys. Rep. **430**, 1 (2006)
26. Y. Shin, M. Saba, T.A. Pasquini, W. Ketterle, D.E. Pritchard, A.E. Leanhardt, Phys. Rev. Lett. **92**, 050405 (2004)
27. Y. Shin, M. Saba, T.A. Pasquini, A.E. Leanhardt, D.E. Pritchard, W. Ketterle, Phys. Rev. Lett. **92**, 150401 (2004)
28. M. Saba, T.A. Pasquini, C. Sanner, A.Y. Shin, W. Ketterle, D.E. Pritchard, Science **307**, 1945 (2005)
29. G.-B. Jo, Y. Shin, S. Will, T.A. Pasquini, M. Saba, W. Ketterle, D.E. Pritchard, Phys. Rev. Lett. **98**, 030407 (2007)
30. G.-B. Jo, J.-H. Choi, T.A. Pasquini, Y.-R. Lee, W. Ketterle, D.E. Pritchard, Phys. Rev. Lett. **98**, 180401 (2007)
31. B. Julsgaard, A. Kozhekin, E.S. Polzik, Nature **413**, 400 (2001)
32. O. Mandel, M. Greiner, A. Widera, T. Rom, T.W. Hansch, I. Bloch, Nature **425**, 937 (2003)
33. A. Sørensen, L.-M. Duan, J.I. Cirac, P. Zoller, Nature **409**, 63 (2001)
34. J. Esteve, C. Gross, A. Weller, S. Giovanazzi, M.K. Oberthaler, Nature **455**, 1216 (2008)
35. B. Wu, Q. Niu, Phys. Rev. A **61**, 023402 (2000)
36. D. Witthaut, E.M. Graefe, H.J. Korsch, Phys. Rev. A **73**, 063609 (2006)
37. N.L. Smith, W.H. Heathcote, G. Hechenblaikner, E. Nugent, C.J. Foot, J. Phys. B: At. Mol. Opt. Phys. **38**, 223 (2005)
38. S. Hofferberth, I. Lesanovsky, B. Fischer, T. Schumm, J. Schmiedmayer, Nature **449**, 324 (2007)
39. S. Hofferberth, I. Lesanovsky, T. Schumm, A. Imambekov, V. Gritsev, E. Demler, J. Schmiedmayer, Nature Phys. **4**, 489 (2008)
40. M.D. Barrett, J.A. Sauer, M.S. Chapman, Phys. Rev. Lett. **87**, 010404 (2001)